Pergamon

Phys. Chem. Earth (C), Vol. 24, No. 4, pp. 407–414, 1999
© 1999 Elsevier Science Ltd
All rights reserved
1464-1917/99/$ - see front matter

PII: S1464-1917(99)00021-5

The Influence of Superathermal Electrons on the Derivation of Coronal Electron Temperatures from Solar Wind Motor Ion Charge States

M. R. Aellig[1], P. Bochsler[2], H. Grünwaldt[3], S. Hefti[2,7], P. Wurz[2], M. Hilchenbach[3], D. Hovestadt[4], F. M. Ipavich[5] and F. Gliem[6]

[1]MIT/Center for Space Research, Rm 37-662B, 77 Massachusetts Avenue, Cambridge, MA 02139, U.S.A.
[2]University of Bern, Sidlestr. 5, CH-3012 Bern, Switzerland
[3]Max-Planck-Institut für Aeronomie, D-37189 Katlenburg-Lindau, Germany
[4]Max-Planck-Institut für Extraterrestrische Physik, D-85740, Garching, Germany
[5]University of Maryland, College Park, MD 20742, U.S.A.
[6]Technische Universität, D-38023 Braunschweig, Germany
[7]Present address: University of Michigan, Ann Arbor, U.S.A.

Received 1 September 1998; revised 20 November 1998; accepted 11 December 1998

Abstract. The CELIAS/CTOF (Charge Time Of Flight) mass spectrometer on board the SOHO mission measures the ionic and elemental composition of minor ions in the solar wind. From density ratios of adjacent charge states of minor ions we derive, consistent with previous measurements of the same type, mean freeze-in temperatures in the slow solar wind in the range between about 1.1×10^6 K and 1.6×10^6 K depending upon the charge states and elements considered. These values are obtained assuming a Maxwellian distribution of the electrons in the inner corona. We assess the influence of suprathermal electrons in the corona upon the density ratios and, subsequently, on the temperature estimates that are drawn from minor ion charge spectra. It was found that only limited amounts of suprathermal electrons are compatible with the charge state observations in the slow solar wind.
© 1999 Elsevier Science Ltd. All rights reserved.

1 Introduction

The charge states of minor ions in the solar wind are a powerful diagnostic tool to detect changes of the electron temperature in the inner corona. Charge state distributions of minor ions in the solar wind are influenced, e.g., by the electron temperature and electron density profiles in the corona, the profile of the speed of the ions in the corona, and the divergence of the expanding flux tubes. However, not only the second moment of the electron distribution, i.e., the electron temperature, but also the higher moments could influence the charge state distribution. Thus, some caution is required when a quantitative link between the observed freeze-in temperatures derived from the minor ion charge state distribution and the electron temperature at the freeze-in location is established.

Whereas for the derivation of freeze-in temperatures from charge state density ratios Maxwellian distributions of the electrons are commonly assumed, there is ample evidence that the solar wind electron distributions have considerable enhancements of the high-energy tail (Feldman et al., 1975; McComas et al., 1992; Ogilvie and Scudder, 1978; Phillips et al., 1995; Pilipp et al., 1987a; Scudder and Olbert, 1979). Remote coronal diagnostics with EUV lines (e.g., Wilhelm et al., 1998) indicate that the electron temperature is lower than estimated from the solar wind minor ions charge states assuming Maxwellian electron distributions. Observations with the SOHO SUMER telescope (Wilhelm et al., 1998) indicate electron temperatures in polar coronal holes below 9×10^5 K in the height range between 1.03 and 1.6 $R_\odot$. Even lower temperatures are observed in polar plumes. Observations of the equatorial streamer belt with SUMER indicate that the electron temperature peaks at 10^6 K with little if any plasma with temperatures in excess of 2×10^6 K (Wilhelm et al., 1997). More recently, Wilhelm et al. (1998), however, reported an electron temperature of approximately 2×10^6 K at 1.1 $R_\odot$ near the equatorial plane. The low electron temperatures, especially in the coronal holes, appear to be in contrast with observations of highly charged ions observed in the corona such as Fe^{12+} (e.g., with SOHO/SUMER) or Fe^{15+} and S^{11+} (SOHO/CDS). At the electron temperatures observed, these highly charged ions would only be present at insignificant levels, if the electron distribution were purely Maxwellian. Increased amounts of suprathermal electrons have been postulated to reconcile the observed low electron temperatures and the observed highly charged ions. Basically, the idea is that the bulk of the electrons causes the comparably low electron temperatures derived from line ratio diagnostics and that the suprathermal electrons cause the highly charged ions observed optically and in the solar wind *in situ*.

We analyze in this paper the influence of departures of the distribution function of the coronal electrons from the commonly assumed Maxwellian distribution on the charge states of solar wind minor ions. Based on measurements of the charge state distributions of oxygen and iron in the slow solar wind we derive upper limits for the amount of suprathermal electrons. Similar studies have been performed by Owocki and Scudder (1983), Bürgi (1987), and Ko et al.

Correspondence to: M. R. Aellig

(1996). These papers, however, deal either with the fast solar wind (Ko et al., 1996), or do not include iron (Bürgi, 1987), or are not based on solar wind measurements (Owocki and Scudder, 1983).

In Section 2 the typically observed charge state spectra of oxygen and iron derived from CELIAS/CTOF data are summarized. Then, we briefly present our description of suprathermal electrons and their impact on the charge states of minor ions. Section 4 describes the parametrization of the coronal outflow chosen. Its results are presented and discussed in Section 5.

2 Typical Charge State Distributions in the Solar Wind

The charge state spectra of oxygen and of iron used for the present study are derived from CELIAS/CTOF data. The evaluation of the densities of the individual oxygen charge states has been given by Hefti (1997) and the analysis of the iron ions is presented by Aellig (1998) and by Aellig et al. (1998). The average density ratios of adjacent charge states and the corresponding equilibrium electron temperatures are summarized in Table 1 for the most prominent charge states of both elements. The data was accumulated between day 150 1996 and day 229 of the same year. The electron temperatures for oxygen and iron are derived from the density ratios of adjacent charge states using the tables of Arnaud and Rothenflug (1985) and Arnaud and Raymond (1992), respectively.

Table 1. Average density ratios of adjacent charge states observed in the slow solar wind with SOHO/CELIAS/CTOF. The electron temperature indicated yields the observed density ratio assuming equilibrium. The equilibrium tables of Arnaud and Rothenflug (1985) and Arnaud and Raymond (1992) are used to calculate the electron temperature.

Ion Pair	Density Ratio	T_e [10^6 K]
O^{7+}/O^{6+}	0.27	1.60
Fe^{9+}/Fe^{8+}	1.55	1.11
Fe^{10+}/Fe^{9+}	1.08	1.11
Fe^{11+}/Fe^{10+}	0.65	1.10
Fe^{12+}/Fe^{11+}	0.53	1.22

The observed density ratios given in Table 1 are used to constrain the distribution of the electrons in the freeze-in region. They are employed to assess the accuracy of the temperature estimates derived from a prescribed outflow profile as discussed in Section 4.

3 Suprathermal Electrons

There are two distinct populations of electrons observed in the solar wind. The distribution function includes thermal or core electrons and suprathermal or halo electrons. It is convenient to describe both populations with Maxwellians with different total densities ($n_{e,c}$, $n_{e,h}$) and temperatures ($T_{e,c}$, $T_{e,h}$). Much literature is available concerning the absolute values of these parameters at 1 AU (e.g., Feldman et al., 1975) and their radial and latitudinal variations (McComas et al., 1992; Ogilvie and Scudder, 1978; Phillips et al., 1995; Scudder and Olbert, 1979). Typical values observed at 1 AU are $T_{e,h}/T_{e,c} \approx 6$ and and $n_{e,h}/(n_{e,c} + n_{e,h}) \approx 5\%$. With Helios, electron distribution functions were measured at heliocentric distances of 0.3 AU (e.g., Pilipp et al., 1987a,b,c)

Another way to describe non-Maxwellian distributions is to use κ-distributions (e.g., Owocki and Scudder, 1983). The parameter κ governs the strength of the high-energy tail. For κ approaching infinity the distribution approaches the Maxwellian distribution. Maksimovic et al. (1997) reported values of κ to range between 2 and 5. Their measurements were done in the solar wind between 1.15 AU and 2.72 AU both in-ecliptic and out-of-ecliptic. Furthermore, they found lower values values of κ in the high-speed streams. Note that, in contrast to the Maxwellian distribution, not all moments exist for κ-distributions. Both descriptions are summarized in Table 2. The characterization of enhanced high-energy tails in the electron distribution is possible with κ-distributions as well as with the sum of two Maxwellian distributions.

The presence of suprathermal electrons alters the ionization rates compared to the case of a Maxwellian electron distribution much stronger than the recombination rates since the ionization has an energy threshold, i.e., the ionization potential of the ion. Recombination, however, is evidently possible with electrons below this energy threshold.

4 Modeling the Charge States using a Prescribed Coronal Outflow

The coronal outflow, i.e., the ion speed u_i, the electron core temperature $T_{e,c}$, and the electron density $n_{e,c}$ are prescribed rather than calculated self-consistently. This procedure was also adopted by Aellig et al. (1997) to estimate the profile of the electron temperature in the inner corona. The following profiles are chosen

$$n_{e,c} = n_{0,c}\, z^a \quad (1)$$

$$T_{e,c} = T_{0,c}\, z^b \quad (2)$$

$$u_i = u_0\, z^{-c} \quad (3)$$

with

$$z = \frac{R_\odot}{R} \quad (4)$$

These profiles are optimized for the inner corona. This means that these profiles have to reproduce the observations, if available, only for heliocentric distances of a few solar radii. Purely radial expansion is assumed for simplicity.

The relative amount of halo electrons is assumed to be constant over heliocentric distance:

$$\frac{n_{e,h}}{n_{e,c}} = c_n \quad (5)$$

Table 2. Comparison of two distinct descriptions of electron distribution functions with suprathermal electrons. See text for references.

	κ-Distribution	Core and halo electrons
Distribution Function	$f_\kappa \propto \left(\frac{m_e}{2\pi k_B T}\right)^{3/2} \times A_\kappa / \left(1 + \frac{E}{(\kappa - 3/2)\, k_B T}\right)^{\kappa+1}$	$f \propto (1-\epsilon)\left(\frac{m_e}{2\pi k_B T_{e,c}}\right)^{3/2} \exp - \frac{E}{k_B T_{e,c}} + \epsilon \left(\frac{m_e}{2\pi k_B T_{e,h}}\right)^{3/2} \exp - \frac{E}{k_B T_{e,h}}$
Observations at 1 AU	$\kappa \approx 2 - 3$[1]	$T_{e,h}/T_{e,c} \approx 6$, $n_{e,h}/n_{e,c}$ a few %
How to get a Maxwellian	$\kappa \to \infty$	$n_{e,h} \to 0, T_{e,h}/T_{e,c} \to 1$
Application (this work)	Equilibrium situation	Parametrization of outflow

[1] between 1.15 and 2.72 AU

Similarly, the ratio of the temperatures of halo and core electrons is assumed to be constant in radial direction:

$$\frac{T_{e,h}}{T_{e,c}} = c_T \tag{6}$$

To calculate the resulting density ratios of adjacent charge states we apply the concept of sudden freeze-in that is described, e.g., by Hundhausen (1972) or by Owocki and Scudder (1983). Basically, as the ions move away from the Sun, the density ratio is established according to the local electron temperature and freezes at the so-called freeze-in radius and remains constant further out. The freeze-in radius is determined from the equality of the characteristic time scales for the charge state modification and the expansion time of the outflow. We assume that within the freeze-in radius the density ratio is given by the equilibrium value

$$\frac{n_i}{n_{i+1}} = \frac{R_{i+1}(T_{e,c}, c_n, c_T)}{C_i(T_{e,c}, c_n, c_T)} \tag{7}$$

where C_i and R_i denote the ionization and recombination rate coefficients of the ion X^{i+}. These rates depend upon the temperature of the core electrons $T_{e,c}$ and the temperature and relative amount of the halo electrons as given by c_T and c_n, respectively. To derive the ionization and recombination rates for the compound electron distributions, the ionization and recombination rates are calculated for the core and halo electrons separately (Arnaud and Raymond, 1992; Arnaud and Rothenflug, 1985) and then weighted with the relative densities of both populations. The drifts of the core and the halo populations (Feldman et al., 1975) are neglected because the drift speeds are small compared with the width of the distributions, i.e., the distributions are only slighlty shifted. This rough estimate is based on the observed drift speeds at 1 AU and the thermal speeds of electrons in the corona based on a temperature of about 10^6 K. The freeze-in radius of an ion pair is derived numerically from the equality between the charge state modification time and the expansion time of the solar wind outflow as described above. The freeze-in radius depends upon the ion pairs considered. For the ion pair O^{7+}/O^{6+} the freeze-in radius is typically below 2 $R_\odot$ whereas for iron the charge states considered freeze between 3 and 4 $R_\odot$.

Four different scenarios of outflow velocities and electron temperature gradients are chosen to estimate the resulting charge states. The parameters of these four scenarios are compiled in Table 3. The parameters of the electron density profile are set based on a fit to data reported by Guhathakurta et al. (1996). The electron temperature gradients cover the range reported by Aellig et al. (1997). In view of the rapid acceleration of the fast solar wind in the polar coronal holes reported, based on measurements with SOHO/UVCS, by Kohl et al. (1997) such a speed profile was included in this survey of the slow solar wind as an extreme case. SOHO/UVCS data provides evidence that no such rapid acceleration is observed for the slow solar wind emerging from the equatorial regions of the corona (L. Strachan, personal communication, 1998). Indeed, in this case considerable acceleration only takes place at larger heliocentric distances than freeze-in of the charge states occurs. Pätzold et al. (1997) inferred the plasma flow speed in the equatorial regions for heliocentric distances between about 5 $R_\odot$ and 30 $R_\odot$ and found that at 5 $R_\odot$ the bulk plasma speed is one third of the speed at 1 AU. Assuming an average speed of 360 km/s for the slow wind at the Earth's orbit this yields an outflow speed of the protons at 5 $R_\odot$ of about 120 km/s. The speeds at 5 $R_\odot$ for the scenarios "average", "flat", and "steep" are consistent with the value reported by Pätzold et al. (1997). The names of these three scenarios refer to the gradient of the electron temperature.

Table 3. Parameters adopted for the four different scenarios. The speed profile of the UVCS scenario is derived from the outflow speed of O^{5+} in a polar coronal hole reported by Kohl et al. (1997). It is included in this analysis of the slow solar wind as an extreme case.

Scenario	n_0 [m^{-3}]	a	b	u_0 [km/s]	c
Average	2.1×10^{14}	4.9	0.49	1.055	2.9
Flat	2.1×10^{14}	4.9	0.35	0.925	2.9
Steep	2.1×10^{14}	4.9	0.71	1.240	2.9
UVCS	2.1×10^{14}	4.9	0.49	1.150	6.0

The density ratios of the ion pairs quoted in Table 1 were simulated on a large grid of the parameters $T_{0,c}$, c_n, and c_T for all four scenarios. The parameter grid is specified in Table 4. From the resulting density ratios the *apparent* freeze-in

Table 4. Grid of parameters $T_{0,c}$, c_n, and c_T. The case of vanishing c_n corresponds to a purely Maxwellian electron distribution.

Parameter	Upper limit	Lower limit	Step
$T_{0,c}$	2.55×10^6 K	0.55×10^6 K	0.1×10^6 K
c_n	0.15	0.00	0.01
c_T	10	2	1

temperatures are derived in order to have a compact description of the ratios even in the presence of suprathermal electrons. The apparent freeze-in temperature has been derived from density ratios in the conventional manner, i.e., assuming the electron distribution to be Maxwellian.

5 Results and Discussion

Before discussing the results for the coronal outflow model using the core/halo description of the electrons, the observed iron charge state distributions are discussed for the case of κ-distributions which is an obvious candidate for electron distribution functions.

We considered the combinations of κ and mean electron energy, given in terms of a temperature T_e, which yield the observed density ratios for the most prominent iron charge states given in Table 1. For a wide range of κ the electron temperatures T_e were calculated from the equilibrium charge state distribution tables for iron for κ-electron distributions reported by Dzifcakova (personal communication, 1997) to yield the measured density ratios. Figure 1 shows the result for the most prominent iron charge states observed in the solar wind. Moderate deviations from the Maxwellian electron distribution, i.e., large values of κ, have only little impact upon the temperature estimate based on the density ratios. This is concluded from the smooth change of the inferred electron temperatures for the four ion pairs in the range $\kappa \geq 7$. The reason for this weak dependence is seen from the electron distribution functions for different values of κ in Figure 2. The ionization potentials of the relevant iron ions are, in this example, far below the energies at which strong enhancements of suprathermal electrons as compared to the purely Maxellian case ($\kappa = \infty$) occur. Thus, for the iron ions considered, an enhancement of the high-energy tail changes the total number of ionizing electrons relatively little. Hence the corresponding ionization rates change only by a small relative amount because only electrons above the threshold given by the ionization potential contribute to the ionization rates. On the contrary, for O^{6+} with an ionization potential of 739 eV, the relative increase of the number of ionizing electrons is stronger with decreasing κ in the example shown in Figure 2.

Considering Figure 1 again, the interpretation using κ functions becomes ambiguous for iron for values of κ below 5. Whereas the higher charge states require very low electron temperatures to explain their observed density ratios, the lower charge states are consistent with the measured density ratios only with increased electron temperatures. For the ex-

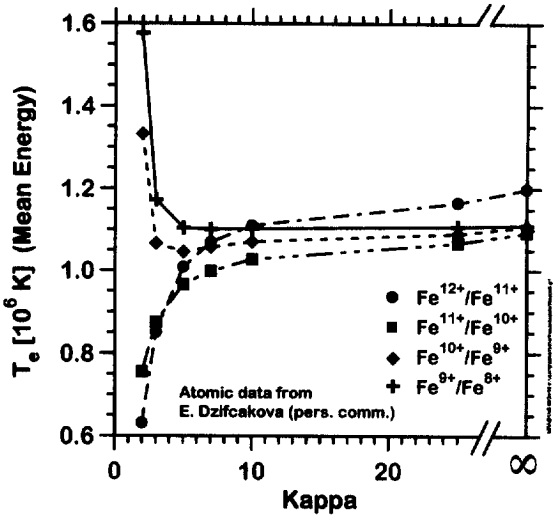

Fig. 1. Combinations of κ and T_e that, in a static situation, yield the average density ratios of iron quoted in Table 1. Given these observed density ratios, the equilibrium charge state distribution tables for iron for κ-electron distribution reported by Dzifcakova (personal communication, 1997) were used to derive T_e for different values of κ. The results for the ion pairs Fe^{9+}/Fe^{8+} (crosses), Fe^{10+}/Fe^{9+} (diamonds), Fe^{11+}/Fe^{10+} (squares), and Fe^{12+}/Fe^{11+} (circles) are given. Lines are plotted to guide the eye. For low values of κ, i.e., for strong deviations from a Maxwellian distribution, the electron temperatures to explain the observed density ratios differ by almost 1×10^6 K which is not compatible with the picture of the iron charge states freezing in at similar heliocentric distances. Furthermore, the electron temperatures required to explain the density ratios of the lower charge states considered are even higher than in the case of a Maxwellian electron distribution.

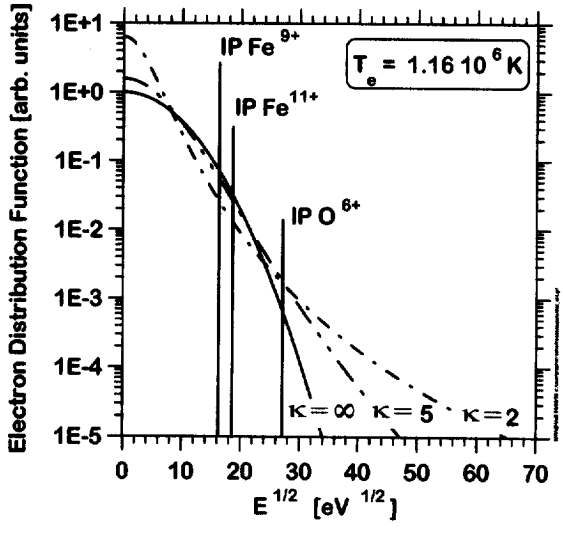

Fig. 2. κ-distribution functions for different values of κ. The mean energy corresponds to a temperature of 1.16×10^6 K in all three cases. Overlaid are the ionization potentials of Fe^{9+}, Fe^{11+}, and O^{6+}.

treme case of $\kappa = 2$ the inferred electron temperatures differ by almost 10^6 K for the different charge states. Even though the freeze-in radii of the different iron ions are not the same, this huge difference is inconsistent with the picture of the most prominent iron charge states freezing at similar distances and therefore at similar temperatures. Furthermore, the electron temperatures required to reproduce the observed density ratios of Fe^{9+}/Fe^{8+} and Fe^{10+}/Fe^{9+} are higher for $\kappa = 2$ than for a Maxwellian distribution of the electrons. As is seen in Figure 2 a considerable reduction of the distribtuion function at thermal energies and above compared to the case of a Maxwellian distribution takes place. This may lead, depending on the ratio of thermal energy of the electrons and the ionization potential involved, to a reduction of the ionization rates (Owocki and Scudder, 1983) and cause the dispersion of T_e shown in Figure 1 for low values of κ. Without debating if the depletion of thermal electrons of the κ-distributions corresponds to reality we note that an inconsistent picture emerges as soon as low values of κ are assumed.

Now, the results for the prescribed coronal outflow with core/halo electron distributions are discussed. The density ratios for the most prominent charge states of iron and oxygen in the solar wind were calculated according to the procedure outlined in Section 4. To have a compact description of the density ratios, the *apparent* freeze-in temperature is derived assuming a purely Maxwellian electron distribution even in cases of enhanced high-energy tails of the electrons. Figure 3 shows a scatter plot of the apparent freeze-in temperatures derived from Fe^{10+}/Fe^{9+} and from O^{7+}/O^{6+}. A total of more than 10,000 cases was calculated with the four scenarios given in Table 3 and the large grid of electron parameters given in Table 4. Whereas the apparent temperature of Fe^{10+}/Fe^{9+} varies from 4×10^5 K to 1.7×10^6 K, i.e., by a factor of four, the apparent freeze-in temperature of O^{7+}/O^{6+} varies by about a factor of almost 10 between 5×10^5 K and 4.5×10^6 K. The larger variation of the oxygen temperature is explained by the higher ionization potential of O^{6+} (739 eV) compared to those of the iron charge states considered (Fe^{8+}: 235 eV; Fe^{9+}: 262 eV; Fe^{10+}: 290 eV; Fe^{11+}: 331 eV). The number of electrons above the ionization potential, and thus the ionization rate, is more sensitive to variations of the shape of the distribution function for larger ionization potentials (see, as an example, Figure 2). Therefore, the ionization balance of O^{7+} and O^{6+} is more sensitive to the contribution of an enhanced high-energy tail of the electrons.

Those cases which yield freeze-in temperatures typically observed at 1 AU lie in the shaded region in Figure 3 and are further analyzed in the following. The apparent oxygen freeze-in temperature $T_{O7/6}$ has to lie within the range of $(1.57 \pm 0.16) \times 10^6$ K and, simultaneously, the iron freeze-in temperature $T_{Fe10/9}$ has to lie within the range $(1.12 \pm 0.07) \times 10^6$ K. We applied the additional criterion that the fraction of halo electrons and temperature ratios in the corona, given by c_n and c_T, may not exceed their typical values observed at 1 AU. We thus consider only cases with $c_T < 8$ and $c_n < 0.07$. In Figure 4 we show the parameters c_n and c_T of the halo electrons that are compatible with the mea-

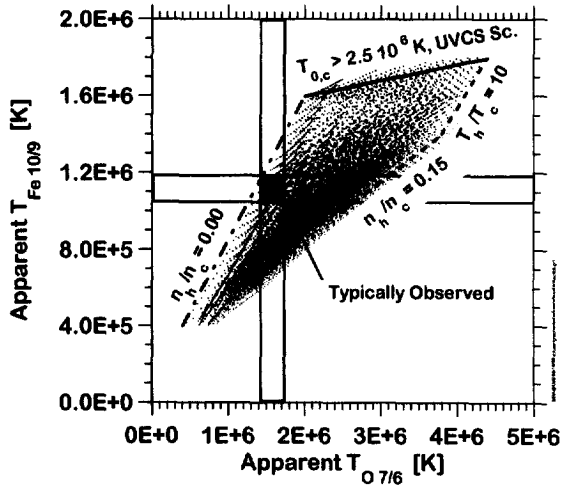

Fig. 3. Scatter plot of the apparent freeze-in temperatures derived from the density ratios O^{7+}/O^{6+} and Fe^{10+}/Fe^{9+} for more than 10,000 cases covering the scenarios in Table 3. The shaded area indicates the range of typically observed freeze-in temperatures in the slow solar wind. The dash-dotted line corresponds to cases where a single Maxwellian distribution describes the electrons. The dashed line corresponds to the case of maximum amount of halo electrons at the highest temperature ratio considered. The solid line represents cases of the scenario "UVCS" with core electron temperature parameters $T_{0,c}$ (see eq. 2) in excess of 2.5×10^6 K.

surements of those parameters at 1 AU and yield, with our parametrization of the coronal outflow, the observed freeze-in temperatures. The amount of halo electrons is comparably low. Either their relative density $n_{e,h}/n_{e,c}$ is low with a large temperature ratio $T_{e,h}/T_{e,c}$, or there are halo electrons present in amounts typically observed at 1 AU with a smaller temperature ratio of 2 or 3.

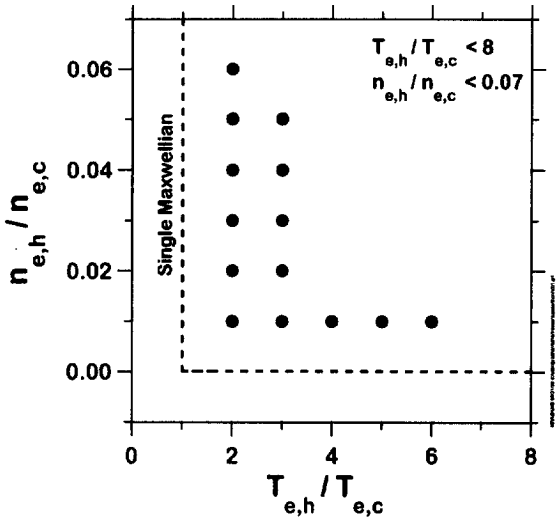

Fig. 4. Parameters of halo electrons that yield the observed apparent freeze-in temperatures (shaded region in Figure 3). The upper limits of the halo electron parameters were set according to the observations at 1 AU ($T_{e,h}/T_{e,c} < 8$; $n_{e,h}/n_{e,c} < 0.07$) as additional selection criteria. The dashed line indicates the parameter combinations that correspond to a purely Maxwellian electron distribution.

Now, we quantify the impact of the departure of the electron distribution from a single Maxwellian distribution on the estimation of the electron temperature with apparent freeze-in temperatures. The difference between the core electron temperature at the freeze-in radius of a given ion pair and the apparent freeze-in temperature derived from this ion pair is taken as a measure for the misinterpretation caused by non-Maxwellian electron distribution functions. Basically, the idea is that the EUV line ratio diagnostics, and thus the relatively low temperatures derived therefrom, are governed by the core electrons, and that the freeze-in temperature derived from the charge states of minor ions might be biased by the presence of halo electrons.

In Figure 5 the core electron temperatures at the freeze-in radii are compared with the apparent freeze-in temperatures derived from the density ratios. In the case of a purely Maxwellian electron distribution both temperatures agree. Deviations from the single Maxwellian electron distribution lead to a difference of these two temperatures. The freeze-in temperature T_{freez} overestimates the true electron temperature $T_{e,c}(R_f)$ in the presence of halo electrons as seen from Figure 5. For oxygen this overestimation is more pronounced than for the iron pair considered. This reflects again

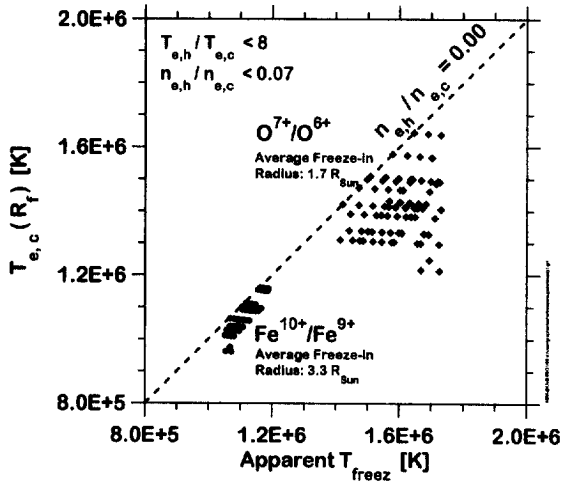

Fig. 5. Scatter plot of the core electron temperature $T_{e,c}$ at the freeze-in radius R_f and the apparent freeze-in temperature T_{freez} for the ion pairs O^{7+}/O^{6+} (diamonds) and Fe^{10+}/Fe^{9+} (circles). The cases consistent with both the iron and oxygen charge states and the electron observations at 1 AU are shown. In the absence of any halo electrons both temperatures are equal (dashed line). The presence of suprathermal electrons increases in all cases the apparent freeze-in temperature T_{freez}. The vertical distance between the symbols and the dashed line indicates the amount by which the core electron temperature is overestimated using the apparent freeze-in temperature the derivation of which assumes a purely Maxwellian distribution of the electrons. The overestimation is much weaker for the iron ions compared to the oxygen ions.

Table 5. Comparison of the average core electron temperature $T_{e,c}$ at the freeze-in radius R_f and the apparent freeze-in temperatures T_f. In addition to the averages, the sample standard deviations are given as well. The difference $\Delta\overline{T}$ between the average core electron temperature $\overline{T_{e,c}(R_f)}$ and the averaged apparent freeze-in temperature $\overline{T_f}$ is considerably smaller for the iron ions than for the oxygen ions. For this compilation, all cases shown in Figure 5 were analyzed.

Ion Pair	$\overline{T_{e,c}(R_f)}$ [10^6 K]	$\overline{T_f}$ [10^6 K]	$\Delta\overline{T}$ [10^6 K]	$\overline{R_f}$ [$R_\odot$]
O^{7+}/O^{6+}	1.44 ± 0.10	1.58 ± 0.09	0.14	1.7 ± 0.2
Fe^{9+}/Fe^{8+}	1.07 ± 0.05	1.09 ± 0.04	0.02	3.5 ± 0.7
Fe^{10+}/Fe^{9+}	1.09 ± 0.05	1.12 ± 0.04	0.03	3.3 ± 0.6
Fe^{11+}/Fe^{10+}	1.11 ± 0.05	1.15 ± 0.04	0.04	3.2 ± 0.6
Fe^{12+}/Fe^{11+}	1.12 ± 0.06	1.16 ± 0.04	0.04	3.1 ± 0.5

the higher sensitivity of the ionization balance of O^{6+} and O^{7+} to enhanced high-energy tails of electrons because of the higher ionization potential of O^{6+} compared to Fe^{9+}. Assuming a purely Maxwellian electron distribution for the derivation of the apparent freeze-in temperatures from the ion pair O^{7+}/O^{6+} can lead to the overestimation of the core electron temperature by no more than 0.5×10^6 K (0.14×10^6 K on average) under the given circumstances. In the case of iron ions Fe^{10+}/Fe^{9+} this bias amounts to less than 0.1×10^6 K (0.03×10^6 K on average). Thus, with the freeze-in temperature derived from this ion pair the core electron temperature at the freeze-in radius can be inferred accurately. As is seen from Table 5, the average bias, i.e., the difference between apparent freeze-in temperature and the core electron temperature at the freeze-in radius, are considerably smaller for the iron freeze-in temperatures considered than for the freeze-in temperature derived from the oxygen ions O^{7+} and O^{6+}.

6 Conclusions

For κ-distributions of the electrons, we have found that with a parameter κ above 5, thus approaching purely Maxwellian electron distributions, according to this model there is no substantial difference between the electron temperature and the observed freeze-in temperatures for the iron ions considered. On the other hand, for lower values of κ, i.e., for stronger deviations from the Maxwellian distribution, an inconsistent picture emerges: To account for the observed values of the density ratios Fe^{11+}/Fe^{10+} and Fe^{12+}/Fe^{11+} given such low values of κ lower electron temperatures than in the case of a Mawellian electron distribution are required whereas the other two density ratios (Fe^{9+}/Fe^{8+}, Fe^{10+}/Fe^{9+}) require higher electron temperatures. Thus only electron κ-distributions with a κ of 5 or more are compatible with the iron charge state spectra observed in the slow solar wind.

Limited amounts of halo electrons in the source regions of the slow solar wind are consistent with the solar wind *in situ* charge states of iron and oxygen within the framework of the present analysis. Either low relative densities $n_{e,h}/n_{e,c}$ of the halo electrons or, for higher relative densities, low temperature ratios $T_{e,h}/T_{e,c}$ are consistent with the data. Given these amounts of suprathermal electrons, the oxygen freeze-in temperatures derived from the charge states O^{6+} and O^{7+} assuming a single Maxwellian electron distribution overestimate, on average, the core electron temperature at the freeze-in radius, i.e., at about 1.7 $R_\odot$, only by 0.14×10^6 K. This bias is much smaller for the iron freeze-in temperatures considered. Due to their comparably low ionization potentials, the most prominent iron charge states observed in the solar wind are robust indicators for the coronal electron temperature at the freeze-in location. From the iron charge states we derive an electron temperature of about 1.1×10^6 K at 3 $R_\odot$ in the source region of the slow solar wind.

Acknowledgements. This work is supported by the Swiss National Science Foundation. CELIAS is a joint effort of five hardware institutions under the direction of MPE (prelaunch) and UBE (post-launch). MPAe was the prime hardware institution for CTOF, UMd was the prime hardware institution for MTOF, UBE provided the entrance systems for both sensors, and TUB provided the DPU. We thank Elena Dzifcakova at the Comenius University, Bratislava, for providing updated equilibrium tables for iron in the presence of electrons with a κ-distribution.

References

Aellig, M. R., *Freeze-in Temperatures and Relative Abundances of Iron Ions in the Solar Wind Measured with SOHO/CELIAS/CTOF*, Ph.D. thesis, University of Bern, 1998.

Aellig, M. R., Grünwaldt, H., Bochsler, P., Hefti, S., Wurz, P., Kallenbach, R., Ipavich, F. M., Hovestadt, D., Hilchenbach, M., and the CELIAS Team, Solar wind minor ion charge states observed with high time resolution with SOHO/CELIAS/CTOF, *ESA SP*, *415*, 27–31, 1997.

Aellig, M. R., Grünwaldt, H., Bochsler, P., Wurz, P., Hefti, S., Kallenbach, R., Ipavich, F. M., Axford, W. I., Balsiger, H., Bürgi, A., Coplan, M. A., Galvin, A. B., Geiss, J., Gliem, F., Gloeckler, G., Hilchenbach, M., Hovestadt, D., Hsieh, K. C., Klecker, B., Lee, M. A., Managadze, G. G., Marsch, E., Möbius, E., Neugebauer, M., Reiche, K. U., Scholer, M., Verigin, M. I., and Wilken, B., Iron freeze-in temperatures measured by SOHO/CELIAS/CTOF, *Journal of Geophysical Research*, *103*, 17215–17222, 1998.

Arnaud, M. and Raymond, J., Iron ionization and recombination rates and ionization equilibrium, *The Astrophysical Journal*, *398*, 394–406, 1992.

Arnaud, M. and Rothenflug, R., An updated evaluation of recombination and ionization rates, *Astronomy and Astrophysics Suppl. Ser.*, *60*, 425–457, 1985.

Bürgi, A., Effects of non-Maxwellian electron velocity distribution functions and nonspherical geometry on minor ions in the solar wind, *Journal of Geophysical Research*, *92*(A2), 1057–1066, 1987.

Feldman, W., Asbridge, J., Bame, S., Montgomery, M., and Gary, S., Solar wind electrons, *Journal of Geophysical Research*, *80*, 4181–4196, 1975.

Guhathakurta, M., Holzer, T. E., and MacQueen, R. M., The large-scale density structure of the solar corona and the heliospheric current sheet, *The Astrophysical Journal*, *458*, 817–831, 1996.

Hefti, S., *Solar Wind Freeze-in Temperatures and Fluxes Measured with SOHO/CELIAS/ CTOF and Calibration of the CELIAS Sensors*, Ph.D. thesis, University of Bern, 1997.

Hundhausen, A. J., *Coronal Expansion and Solar Wind*, Springer, 1972.

Ko, Y.-K., Fisk, L., Gloeckler, G., and Geiss, J., Limitations on suprathermal tails of electrons in the lower solar corona, *Geophys. Res. Letters*, *23*, 2785–2788, 1996.

Kohl, J., Noci, G., Antonucci, E., Tondello, G., Huber, M., Gardner, L., Nicolosi, P., Strachan, L., Fineschi, S., Raymond, J., Romoli, M., Spadaro, D., Panasyuk, A., Siegmund, O., Benna, C., Ciaravella, A., Cranmer, S., Giordano, S., Karovska, M., Martin, R., Michels, J., Modigliani, A., Naletto, G., Pernechelle, C., Poletto, G., and Smith, P., First results from the SOHO ultraviolet coronograph spectrometer, *Solar Physics*, *175*, 631–644, 1997.

Maksimovic, M., Pierrard, V., and Riley, P., Ulysses electron distributions fitted with Kappa functions, *Geophys. Res. Letters*, *24*, 1151–1154, 1997.

McComas, D., Bame, S., Feldman, W., Gosling, J., and Phillips, J., Solar wind halo electrons from 1–4 AU, *Journal of Geophysical Research*, *19*, 1291–1294, 1992.

Ogilvie, K. and Scudder, J., The radial gradients and collisional properties of solar wind electrons, *Journal of Geophysical Research*, *83*, 3776–3782, 1978.

Owocki, S. P. and Scudder, J. D., The effect of a non-Maxwellian electron distribution on oxygen and iron ionization balances in the solar corona, *The Astrophysical Journal*, *270*, 758–768, 1983.

Pätzold, M., Tsurutani, B., and Bird, M., An estimate of the large-scale solar wind density and velocity profiles in a coronal hole and the coronal streamer belt, *Journal of Geophysical Research*, *102*, 25,151–24,160, 1997.

Phillips, J., Bame, S., Gary, S., Gosling, J., Scime, E., and Forsyth, R., Radial and meridional trends in solar wind thermal electron temperature and anisotropy: Ulysses, *Space Sci. Rev.*, *72*, 109–112, 1995.

Pilipp, W., Miggenrieder, H., Montgomery, M. D., Mühlhäuser, K.-H., Rosenbauer, H., and Schwenn, R., Characteristics of electron velocity distribution functions in the solar wind derived from the helios plasma experiment, *Journal of Geophysical Research*, *92*, 1075–1092, 1987.

Pilipp, W., Miggenrieder, H., Montgomery, M. D., Mühlhäuser, K.-H., Rosenbauer, H., and Schwenn, R., Unusual electron distribution functions in the solar wind derived from the helios plasma experiment: Double-strahl distributions and distributions with an extremely anisotropic core, *Journal of Geophysical Research*, *92*, 1093–1101, 1987.

Pilipp, W., Miggenrieder, H., Mühlhäuser, K.-H., Rosenbauer, H., Schwenn, R., and Neubauer, F. M., Variations of electron distribution functions in the solar wind, *Journal of Geophysical Research*, *92*, 1103–1118, 1987.

Scudder, J. and Olbert, S., A theory of local and global processes which affect solar wind electrons 2. Experimental support, *Journal of Geophysical Research*, *84*, 6603–6620, 1979.

Wilhelm, K., Lemaire, P., Curdt, W., Schühle, U., Marsch, E., Poland, A. I., Jordan, S. D., Thomas, R. J., Hassler, D. M., Huber, M. C. E., Vial, J. C., Kühne, M., Siegmund, O. H. W., Gabriel, A., Timothy, J. G., Gredwing, M., Feldman, U., Hollandt, J., and Brekke, P., First results of the SUMER telescope and spectrometer on SOHO, *Solar Physics*, *170*, 75–104, 1997.

Wilhelm, K., Marsch, E., Dwivedi, B. H., Hassler, D. M., Lemaire, P., Gabriel, A. H., and Huber, M. C. E., The Solar Corona Above Polar Coronal Holes as Seen by SUMER on SOHO, *The Astrophysical Journal*, *500*, 1023–1038, 1998.